 Human Molecular Genetics, 2002, Vol. 11, No. 9 1005–1016

Murine model of autosomal dominant retinitis pigmentosa generated by targeted deletion at codon 307 of the *rds*–peripherin gene

Niamh McNally[1,*], Paul F. Kenna[1], Derrick Rancourt[2], Tanweer Ahmed[3], Alan Stitt[4], William H. Colledge[5], David G. Lloyd[6], Arpad Palfi[1], Brian O'Neill[1], Marian M. Humphries[1], Peter Humphries[1] and G. Jane Farrar[1]

[1]The Ocular Genetics Unit, Trinity College Dublin, Dublin 2, Ireland, [2]Southern Alberta Cancer Research Centre, Department of Biochemistry and Molecular Biology, University of Calgary, Alberta, Canada T2N 4N1, [3]School of Biochemistry, University of Leeds, Leeds LS2 9JT, UK, [4]Department of Ophthalmology, The Queen's University of Belfast, Belfast, UK, [5]Department of Physiology, University of Cambridge, UK and [6]Pharmaceutical Chemistry Department, School of Pharmacy, Trinity College Dublin, Dublin 2, Ireland

Received January 15, 2002; Revised and Accepted March 7, 2002

We introduced a targeted single base deletion at codon 307 of the *rds*–peripherin gene in mice, similar mutations being known to cause autosomal dominant retinitis pigmentosa (RP) in man. Histopathological and electroretinographic analysis indicate that the retinopathy in mice homozygous for the codon 307 mutation appears more rapid than that in the naturally occurring null mutant, the *rds*$^{-/-}$ mouse, suggesting that the *rds*-307 mutation displays a dominant negative phenotype in combination with that due to haplosufficiency. RP is the most prevalent cause of registered visual handicap in those of working age in developed countries, the 50 or so mutations so far identified within the *RDS*–peripherin gene accounting for up to 10% of dominant cases of the disease. Given the sequence homologies that exist between the murine *rds*–peripherin and the human *RDS*–peripherin gene, this disease model, the first to be generated for peripherin-based RP using gene targeting techniques, should in principle be of value in the work-up in mice of therapeutics capable of targeting transcripts derived from the human gene.

INTRODUCTION

Retinitis pigmentosa (RP), an hereditary degenerative disease of the retina involving progressive death of rod and subsequently cone photoreceptor neurons, is a prevalent cause of registered visual handicap among working populations globally (1,2). An impediment to the development of genetically based therapeutics for this condition is the genetic heterogeneity associated with it. The disease segregates in families according to mendelian dominant, recessive, X-linked recessive, mitochondrial or digenic modes, up to 30 genes having so far been implicated in the etiology of the condition (http://www.sph.uth.tmc.edu/retnet/). Among autosomal dominant forms of RP, mutations within the rhodopsin and RDS–peripherin genes, encoding respectively the primary photoreactive pigment of rod photoreceptors and a structural component necessary for integrity of photoreceptor outer segment disc membranes, are the most frequent, accounting for up to 30% of dominant RP cases (3–5). A combined total of approximately 200 mutations have so far been characterized in autosomal dominant RP within the rhodopsin and RDS–peripherin genes (http://www.sph.uth.tmc.edu/retnet/, http://www.retina-international.com). The heterogeneity inherent in RP presents a significant barrier to the design and development of therapeutics. This is particularly apparent in dominant forms of RP, where it will not be economically viable to develop therapeutics targeting individual dominant-negative mutations. In this regard, it is notable that mutation-independent techniques that target the primary genetic defect but overcome such heterogeneity have been developed (6–9).

Peripherin is a transmembrane protein of outer segment disc membranes of photoreceptor cells, and is located towards the periphery of the discs – hence its name. In rod photoreceptors, peripherin can interact with Rom1 (rod outer segment protein 1) to form heterodimers providing disc stability (10–13). A naturally occurring rds–peripherin null mutation in the mouse causes a retinal degeneration termed 'retinal degeneration slow', or rds (14–16). In the current study, a single base pair deletion at codon 307 of the rds–peripherin gene was introduced into mice by homologous recombination in ES cells. In humans, the

*To whom correspondence should be addressed. Tel: + 353 1 6082484; Email: mcnallyn@tcd.ie

RDS-307 mutation results in a slowly progressive form of autosomal dominant RP (17). The human mutation causes a frameshift and as a result creates a stop codon after a further 16 triplets. The expected protein is therefore 26 amino acids shorter than human wild-type RDS–peripherin. The clinical profile of the human disease involves a decline in visual acuity, loss of peripheral vision in the fifth decade of life and onset of night blindness in the sixth decade (17). Thus, the disease caused by the 307 mutation is relatively mild. The frameshift brought about in the mouse genome by the 1 bp deletion at codon 307 is predicted to result in alteration of the last 40 amino acids of the C terminus of the protein and the addition of an extra 11 amino acids. The current study details observations on the disease phenotype produced as a result of introduction of the 307 modification. In heterozygous and homozygous rds-307 mice, the induced retinopathy appears to be more rapid when compared with $rds^{+/-}$ or $rds^{-/-}$ mice, the majority of the outer nuclear layer (ONL) of the retina being lost in rds-307 heterozygotes at 10 months, while in rds-307 homozygotes almost complete loss of ONL and rod and cone photoreceptor function occurs by about 4 months of age. These observations suggest that the targeted modification introduced into the rds–peripherin gene results in a dominant-negative effect. In this context, it is of interest to note that in previous studies, a combination of effects of dominant-negative mutations (P216L) and haplosufficiency have been documented (18). rds-307 mice, however, represent the first targeted modification of the rds-peripherin gene that contains a dominant mutation akin to that observed in the human disease. This animal model will be of value in deciphering disease mechanisms involved in peripherin-linked retinal degenerations, and, in view of the close sequence homologies between the mouse and human genes, will be of value in the assessment of therapeutics targeting human RDS–peripherin transcripts.

RESULTS

Histopathology of retinas of rds-307 mice

Retinas from rds-307 heterozygous mice were studied by light microscopy at 2, 6, 10 and 12 months of age (Fig. 1). Nine or ten rows of photoreceptor nuclei were present in the central retina at 2 months, four or five rows at 6 months, three or four rows at 10 months and two or three rows at 12 months. The degeneration in rds-307 heterozygotes therefore appears to be more rapid than that observed in $rds^{+/-}$ null heterozygotes, which retained six or seven rows of nuclei at 9 months (19) and maintained approximately half the normal photoreceptor cell population at 9–10 months (20). Photoreceptor degeneration at 1, 2, 3 and 4 months among wild-type control mice, homozygous rds-307 mice and $rds^{-/-}$ mice was also compared by counting rows of photoreceptor nuclei in the outer nuclear layer. Homozygous rds-307 mice show a relatively rapid photoreceptor degeneration, with only four or five rows of nuclei remaining at 1 month and essentially a single row at 4 months (Fig. 2). The $rds^{-/-}$ mouse retinas analyzed retained eight or nine rows of photoreceptor nuclei at 1 month and three or four rows at 4 months (Fig. 2). The findings in $rds^{-/-}$ homozygotes in the current study are consistent with previously published observations (14).

Transmission electron microscopy (EM) was undertaken on heterozygous rds-307 mice at 6 and 10 months of age and on homozygous rds-307 mice at 5 weeks of age (Fig. 3). Mice heterozygous for the codon 307 mutation showed a marked reduction in rod photoreceptor cell numbers in comparison with that observed in retinas from wild-type mice. The ONL was four or five nuclei in thickness at 6 months (consistent with data obtained from light microscopy) and there was evidence of ongoing depletion of these cells over time (Fig. 3B,E). Remaining cells still retained inner segments, although the membranous discs of the outer segments were severely disrupted in number and configuration (compare Fig. 3C with 3A). Outer segments were short and somewhat segmented into whorl-like structures (see Fig. 3D). The pigment epithelium (RPE) appeared to be still phagocytosing these membranes, although there were fewer phagosomes observed than in wild-type retinas. This observation is different to that found in $rds^{-/-}$ mice, where typically many phagosomes are visible (21). The inner retina of heterozygote rds-307 mice was ultrastructurally normal in appearance. Overall, there was little obvious difference between 6- and 10-month heterozygous rds-307 mice in

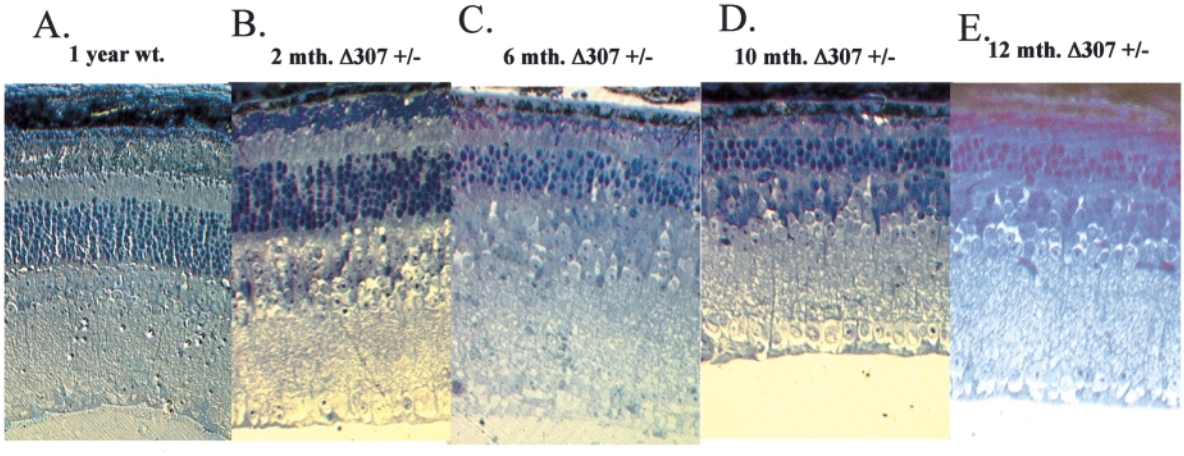

Figure 1. Light micrographs of retinal sections of 1-year-old wild-type mouse (A) and 2-, 6-, 10- and 12-month-old heterozygotes for the rds-307 mutation (B–E), respectively. Magnification 400× .

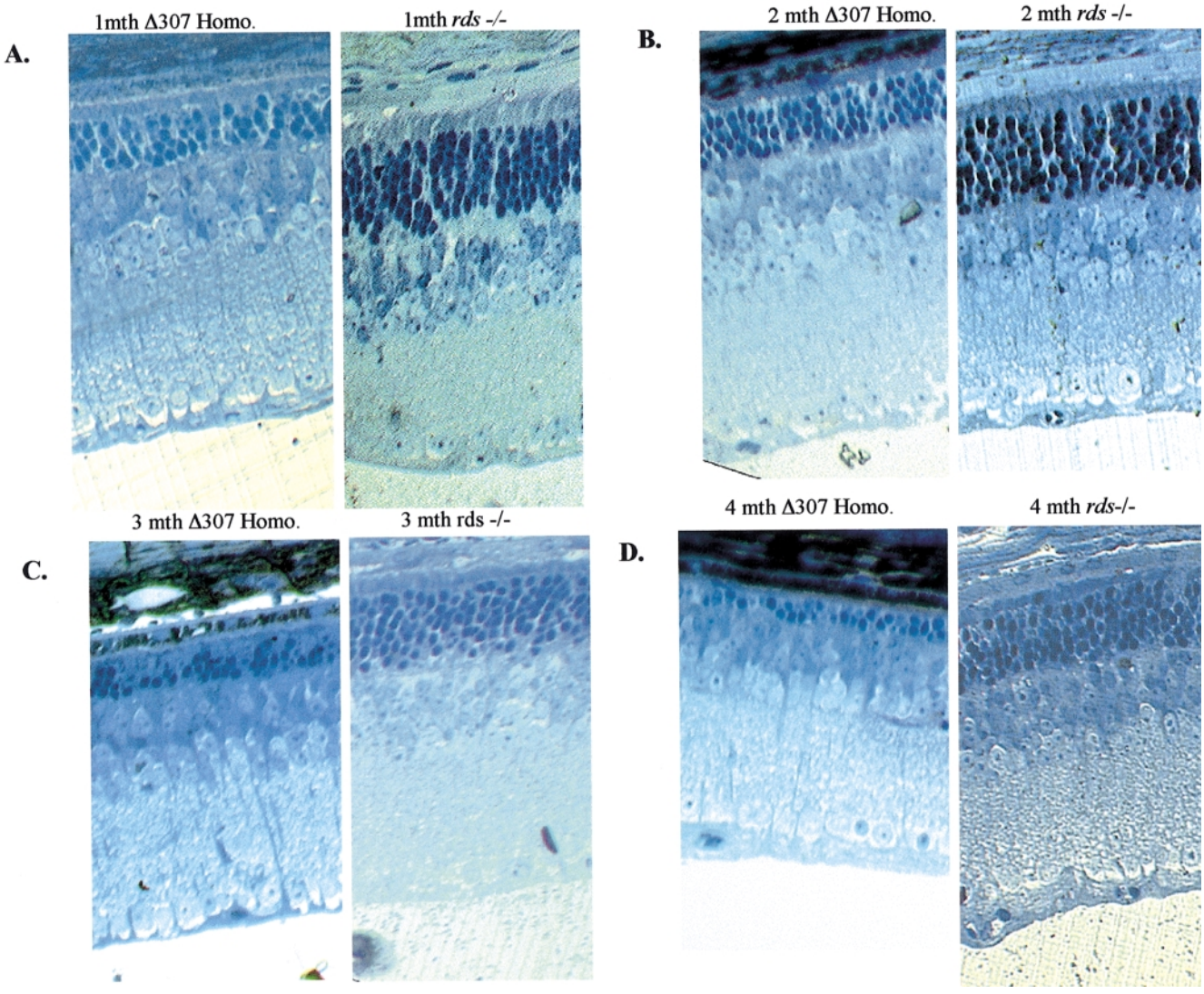

Figure 2. Comparison of light micrographs of retinal sections from rds-307 homozygotes and rds$^{-/-}$ homozygotes at 1, 2, 3 and 4 months of age, respectively. Magnification 400× .

terms of outer retinal abnormalities, although, clearly, retinas from 10 month rds-307 heterozygotes demonstrated a further reduced ONL (three or four nuclei thick).

Mice homozygous for the codon 307 mutation exhibited severe loss of rod photoreceptors with the ONL being reduced to three or four nuclei in thickness at 5 weeks (Fig. 4A). The inner segments (IS) of the remaining cells were present, although the outer segments were universally absent (Fig. 4B) from both rods and cones. The external limiting membrane and Müller cell processes remained intact (Fig. 4C). The RPE was largely normal, although there was little evidence that these cells had recently engulfed rod outer segments (ROS), since few phagosomes were observed throughout this layer (Fig. 4A,B). Apoptotic cell death was apparent in the ONL at 5 weeks, as evidenced by numerous apoptotic bodies present in this region of the retina (Fig. 4D). The outer plexiform layer (OPL) was disrupted, but beyond this layer the inner retina was largely normal in appearance.

Analysis of rds-307 transcripts in mouse retinas

Confirmation of the presence of the codon-307 mutation in targeted rds-307 mice was also obtained by analyzing transcripts from retinas of rds-307 mice and wild-type mice. RNA was extracted from retinas of heterozygous and homozygous rds-307 mice and from wild-type control mice, and used to generated cDNA via RT–PCR. The resulting PCR products were analyzed in an ABI 310 genetic analyzer. Figure 5 demonstrates that two populations of peripherin transcript were present in heterozygous rds-307 mouse retinas. The analysis provides evidence that one of the peripherin transcripts is a single base smaller in size than the other transcript, indicating the presence of both wild-type and rds-307 transcripts in retinas from rds-307 heterozygotes. Similarly, homozygous rds-307 mouse retinas were found to contain only rds-307 transcripts, while control mice had only wild-type peripherin transcripts in their retinas. It should also

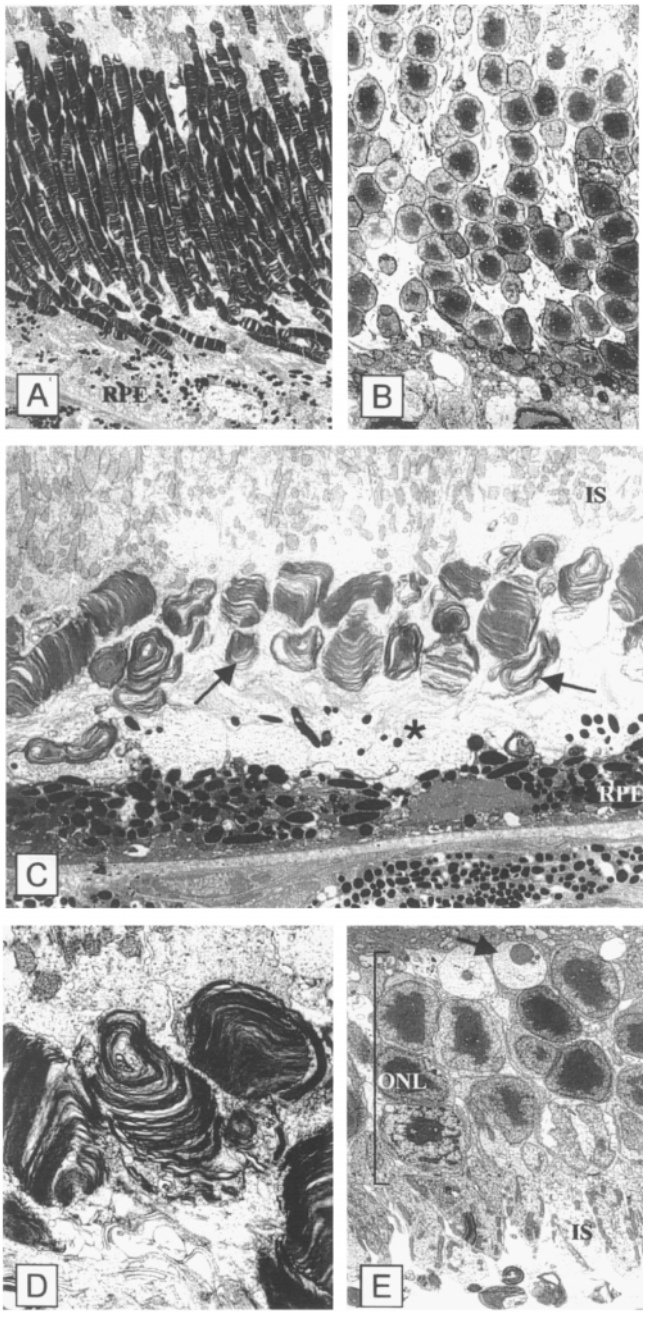

Figure 3. Electron micrographic analysis of wild-type mouse retinas showing normal morphology of photoreceptor outer segments (A) and full-thickness ONL (B). (C) rds-307 heterozygotes at 10 months of age, with arrow and (*) showing disruption of outer segments and electron-lucent membranous material at the level of the subretinal space between outer segments of the apical plasma membrane of the RPE, respectively. (D) Higher magnification shows the whorl-like configuration of the outer segments in a 6-month-old rds-307 heterozygote. (E) The ONL for a 10-month-old rds-307 heterozygote; the arrow indicates further depletion through apoptotic death. Magnification: (A) × 500; (B) × 1500; (C) × 2500; (D) × 8250; (E) × 2500.

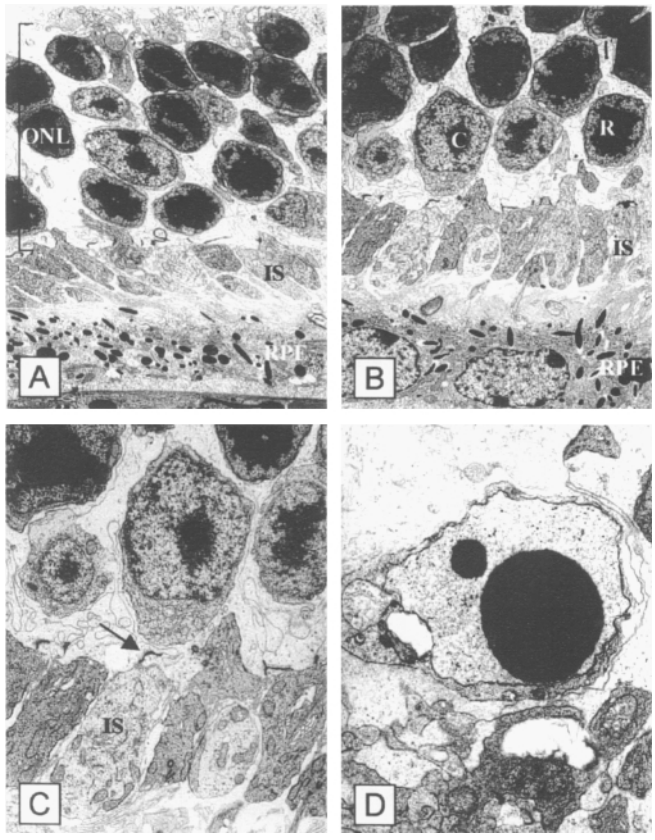

Figure 4. Ultrastructural assessment of the retina in mice homozygous for the rds-307 mutation at 5 weeks. (A) Comprehensive and widespread loss of photoreceptors, with ONL three or four nuclei in thickness. Photoreceptors have no outer segments, and the photoreceptor inner segments (IS) are adjacent to apical plasma membrane of the RPE. (B) A mixture of rods (R) and cones (C) remain, although it would appear that the cones have survived preferentially in these retinas. The RPE appears normal, although there is little evidence of recent phagosomes in their cytoplasm. (C) The cell shows typical cone photoreceptor morphology, with slightly larger, more electron-lucent nuclei in comparison with rod cells. The cone IS appear normal, although no outer segments are visible. Desmosomes forming the external limiting membrane are also obvious (arrow). (D) Apoptotic cell death is an ongoing process in these eyes, as indicated by numerous apoptotic bodies in the region of the ONL. This dying cell shows marked condensation of nuclear chromatin a hallmark of programmed cell death. Magnification: (A) × 2500; (B) × 2500; (C) × 4000; (D) × 8000.

be noted that transcripts from the mutant allele are present at 60–65% of levels derived from the wild-type allele. These observations are in agreement with data in recent reports by Nagy and colleagues (22), in which levels of transcript derived from genes containing neomycin resistance cassettes inserted into introns are generally downregulated by up to 40%.

Electroretinographic analysis

The electroretinogram (ERG) is a mass potential recorded from the corneal surface of the eye. The ERG generated by a brief flash consists of an initial cornea-negative a-wave, the early portion of which reflects phototransduction activity of rod and cone photoreceptors and the later portion of which reflects inner retinal negative components. The a-wave is followed by components that arise from second-order neuronal activity. Most prominent of these is the b-wave, a cornea-positive waveform.

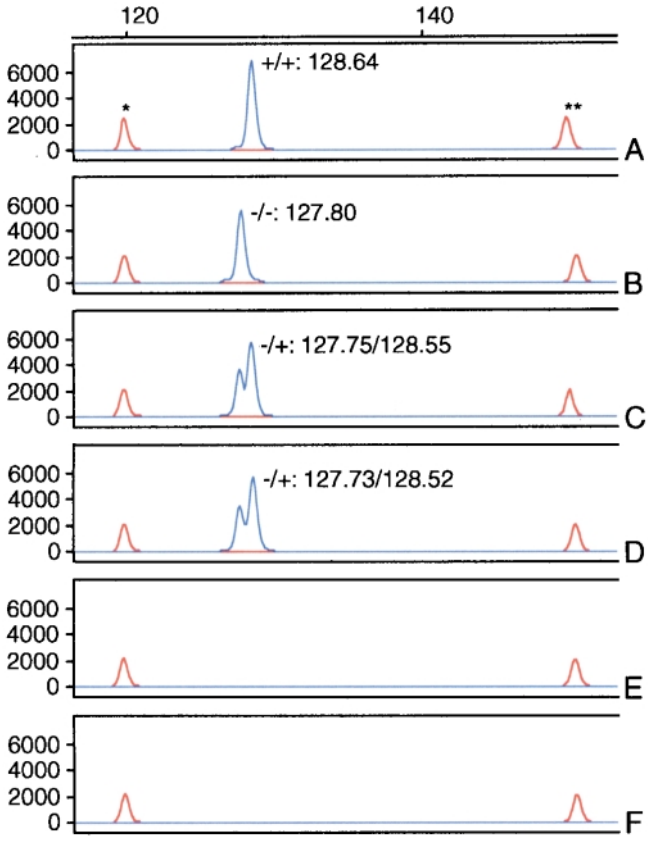

Figure 5. Analysis of rds-307 transcripts in mouse retinas. * 120 bp size marker; ** 150 bp size marker (A) Animal 1, homozygous wild-type. (B) Animal 2, homozygous Δ307 deletion. (C) Animal 3, heterozygous. (D) Animal 4, heterozygous. (E) Animal 3, heterozygous, control (Omniscript reverse transcriptase omitted). (F) Animal 4, heterozygous, control (Omniscript reverse transcriptase omitted). Note that the expected sizes are 131 and 130 bp, for wild-type and the Δ307 deletion, respectively. However size-calling is not absolute; the corresponding sizes are approximately 128.6 and 127.7 bp for wild-type and the Δ307 deletion, respectively.

No convincing rod-isolated responses could be elicited from homozygous rds-307 mice even at 1 month of age. Homozygous rds-307 mice showed very significant attenuation of maximal-intensity b-wave amplitudes from an early age. The responses recorded from 2-, 3- and 4-month old mice are shown in Figure 6. The corresponding amplitudes from age-matched rds$^{-/-}$ mice are shown in the same figure, demonstrating that the phenotype in rds-307 mice is noticeably more severe. Whilst a small-amplitude b-wave could still be recorded from a 4-month-old rds$^{-/-}$ animal, no such peak could be recorded from a 4-month-old rds-307 homozygote.

Figure 7 illustrates the ERG responses recorded from 6- and 10-month-old rds-307 heterozygotes. The rod-isolated responses generated by a 6-month-old rds-307 heterozygote compare well with those of a wild-type mouse. The mixed rod/cone response of the dark-adapted eye of this animal to a maximal-intensity flash presented in the dark-adapted state showed significant reduction in both a-wave and b-wave amplitudes, as did the cone-isolated responses to single flash. By 10 months of age, there had been a significant deterioration in rod-isolated b-wave amplitudes, as well as in maximal dark-adapted responses and cone-isolated responses. The time course of the ERG amplitude deterioration mirrored that seen in histology.

DISCUSSION

In designing a therapeutic strategy for a disease such as autosomal dominant RP, it is important to establish whether the disease pathology is caused by haploinsufficiency of the wild-type gene product or a dominant-negative effect(s) of mutant protein or alternatively a combination of both mechanisms. To simulate the human condition in an animal model, a targeting approach in mouse ES cells has been adopted, enabling introduction of a subtle mutation (a 1 bp deletion at codon 307) into the endogenous mouse rds–peripherin gene. The pathology

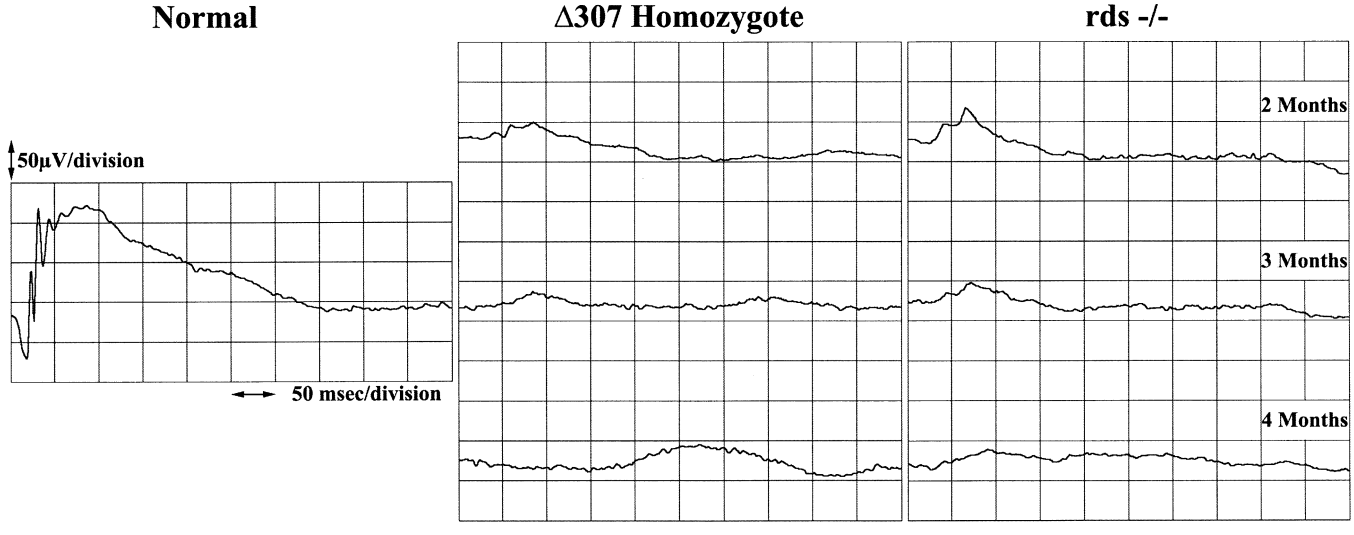

Figure 6. Mixed rod/cone electroretinographic responses of 2-, 3- and 4-month-old dark-adapted mice to a maximal-intensity flash. Note the gross attenuation of the b-wave in both Δ307 homozygotes and rds$^{-/-}$ mice, the attenuation being greater in Δ307 animals.

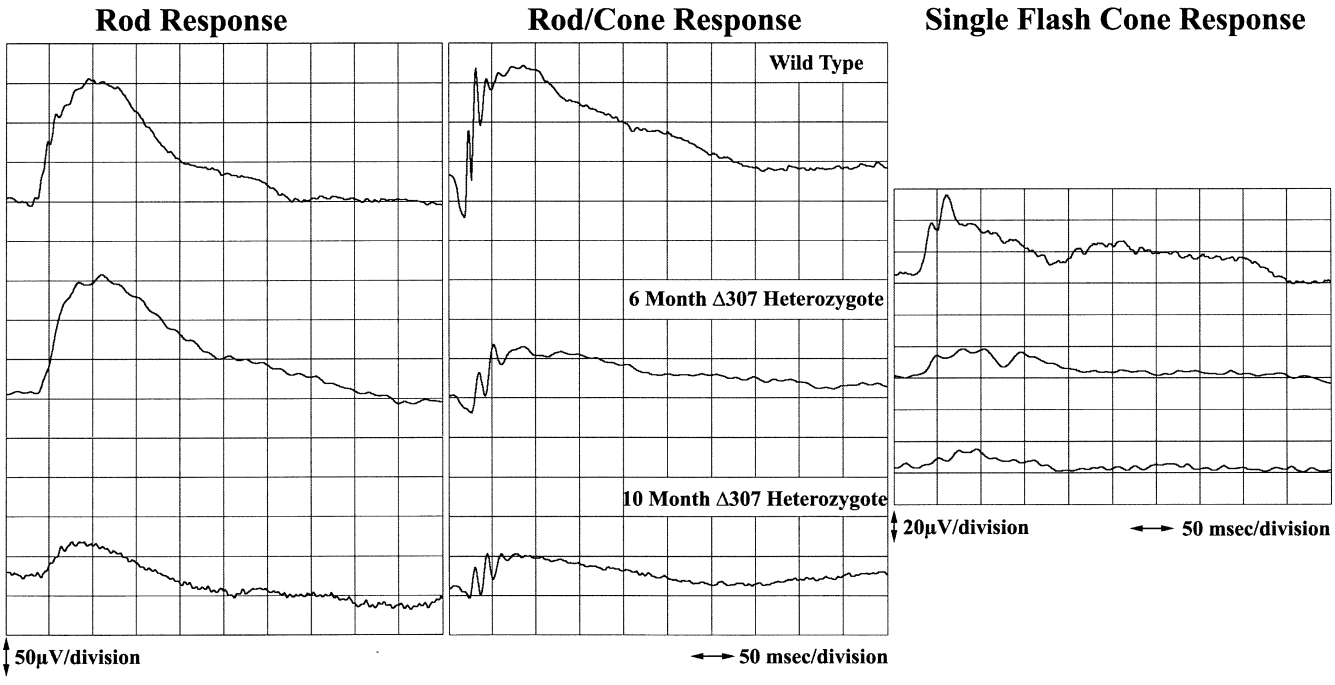

Figure 7. Rod-isolated, mixed rod/cone and pure cone responses from 6- and 10-month-old rds-307 heterozygotes. Relatively normal rod responses persist up to 6 months in heterozygotes, but diminish significantly by 10 months. Mixed rod/cone responses are attenuated at 6 months, as are the pure cone amplitudes, with further deterioration noted by 10 months.

observed in the resulting rds-307 mice suggests that disease pathology is due to the presence of mutant peripherin protein and not simply an absence of wild-type protein, since the disease appears to be more severe in homozygous rds-307 mice than in homozygous rds$^{-/-}$ null mice (see Figs 1 and 2).

It is also of interest to speculate on possible mechanisms by which the codon 307 mutation in the rds–peripherin gene may exert a dominant-negative effect. It has been previously well established that peripherin protein is involved in maintaining the integrity of the structure of photoreceptor disc membranes (10,23,24). In this regard, it is worth noting that evidence has been obtained to suggest that the C terminus of the peripherin protein may be involved in ROS membrane fusion. Studies in vitro have suggested that a 15-amino-acid sequence within the C terminus of the protein (at positions 313–327) is involved in aiding ROS membrane fusion (26). Notably, this amino acid sequence is predicted to be altered in the mutant rds-307 protein, and hence it is possible that the ability of the mutant protein to promote membrane fusion may be compromised. In addition, preliminary studies carried out by D. Papermaster and colleagues in Xenopus laevis suggest that the C-terminus of peripherin protein promotes outer segment localization (25), and therefore a similar situation might pertain in the case of mouse peripherin. A role for peripherin in maintaining the flattened vesicle morphology characteristic of photoreceptor outer segments has been suggested, and two rds–peripherin mutants (P216L and C156Y) have been shown to be unable to flatten membrane vesicles in vitro (27). Future studies could be carried out on the rds-307 protein to see if this is the cause of the dominant-negative effect observed in this newly generated animal model.

It is notable that the predicted C-terminus of the mutant mouse rds-307 protein possesses a significantly higher ratio of basic amino acids and a lower number of acidic amino acids than the wild-type protein, which has a direct effect on pI (8.32 versus 9.34) and hence protein folding in vivo (Fig. 8). Other factors that may be of significance are the presence of and the relative positions of proline residues in the mutant protein: in general, such residues introduce a 45° kink in the amino acid backbone. In addition, the increased number of non-polar amino acids would induce a larger bulk volume. The introduction of an additional cysteine residue in the mutant may possibly facilitate aberrant bond formation with cysteine residues present in the large intradiscal domain of the protein. To investigate possible divergence in the secondary structure of the mutant protein from the wild-type, both wild-type and mutant sequences were submitted to the Jpred secondary structure prediction utility at EBI (28). Notably, differences in the predicted helical structures for the C terminus of the mutant and wild-type proteins were obtained (Figs 9 and 10). It is of interest to note that predicted changes in mutant as opposed to normal proteins in the mouse are also likely to be present in mutant human peripherin, specifically, a higher ratio of basic amino acids, pI (8.4 versus 9.16) the presence of proline residues and an additional cysteine residue. Therefore, pathological disease mechanisms, at the molecular level, may be similar in both murine and human retinas.

The development of therapeutics for autosomal dominant RP caused by mutations within the RDS–peripherin gene is severely complicated by the extensive genetic heterogeneity inherent in this group of conditions. The complexity and fragility of photoreceptor neurons is further highlighted by the

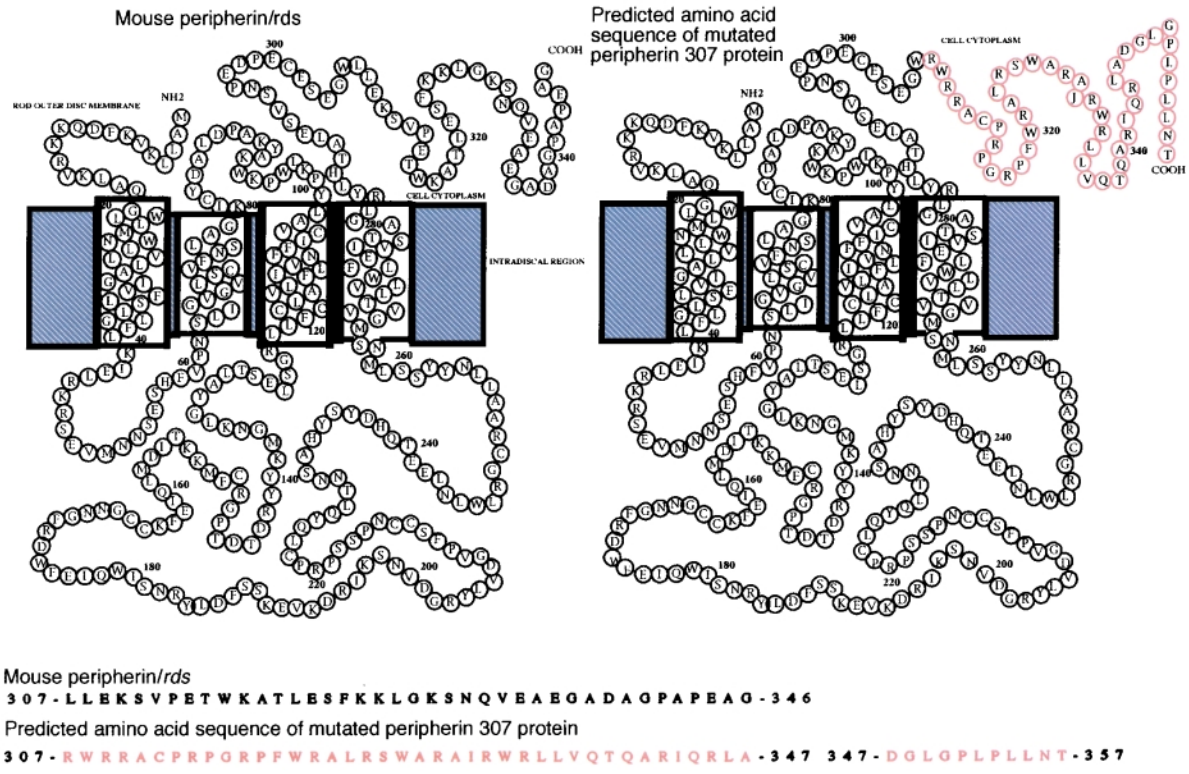

Figure 8. Topological model of normal rds–peripherin and mutated Δ307 rds–peripherin proteins based on findings published by Connell et al. (16), Bascom et al. (11) and Molday (24). The predicted amino acid sequence of the mutated protein is highlighted in red.

```
301-------311-------321-------331-------341---- :
CESEGWLLEKSVPETWKATLESFKKLGKSNQVEAEGADAGPAPEAG : OrigSeq

------HHHHHHHHHHHHHHHHHHH-----EEE------------ : dsc
------HHH-----HHHHHHHHHHHH------E------------- : jalign
-----EEE----HHHHHHHHHHHHH-----HHHHHH---------- : jfreq
-----------HHHHHHHHHHHHHH-------------------- : jhmm
------E-----HHHHHHHHHHHHHH-------------------- : jnet
----------HHHHHHHHHHHHHH--------------------- : jpssm
H----HHHH---HH--H--HHHHH---------------------- : mul
----HHHHE--HHHHHHHHHHHHHH--------------------- : phd
-----EEE---HHHHHHHHHHHHHH--------------------- : pred
-HHHHHH---------------------------------------- : zpred

------E----HHHHHHHHHHHHHH--------------------- : Jpred

301-------311-------321-------331-------341-------351---- :
CESEGWRWRRACPRPGRPFWRALRSWARAIRWRLLVQTQARIQRLADGLGPLPLLNY : OrigSeq

------HHH-------HHHHHHHHHH------------------------------ : jalign
------EE--------HHHHHHHHHH-------HEE-E------------------- : jfreq
------EE-----HHHHHHHHHHHHH------------------------------ : jhmm
------EE----HHHHHHHHHHHHH-------EE-----HHHHH------------ : jnet
-----------HHHHHHHHHHHHHHHHH-EEEEEEEHHHHHHHHHH---------- : jpssm
H-----HHH----------HHHHHH--------------------------------- : mul
------EEE---HHHHHHHHHHHHHH------------------------------ : phd
---------------HHHHHHHHHHHHHHHHHHHHHHHHHHHHHHHH---------- : pred
---------------------------------------------------------- : zpred

------EE-----HHHHHHHHHHHHH------------------------------ : Jpred
```

Figure 9. Jpred output for C-terminal divergent sequences. This figure focuses on the key region of divergence in amino acid sequences at the C termini from residue 301 in both proteins, and illustrates the Jpred output of predicted secondary structure for both proteins (H, helix; E, extended; −, loop). It can be clearly seen that for the mutant protein, 4 of the 10 prediction engines queried report a higher helical (or more highly structured) content for the mutant over the wild-type in the C-terminal region. To verify this trend, the C-terminal sequences for the divergent regions (301−) were submitted to the agadir helical content prediction engine at EMBL (2–6). The percentage prediction of helical content for the mutant terminal fragment is 8.07%, compared with a 1.31% helical content predicted for the wild-type protein with this method. Following this prediction, the same sequence fragments were submitted to the ProtScale conformational analysis engine for comparison (37–42).

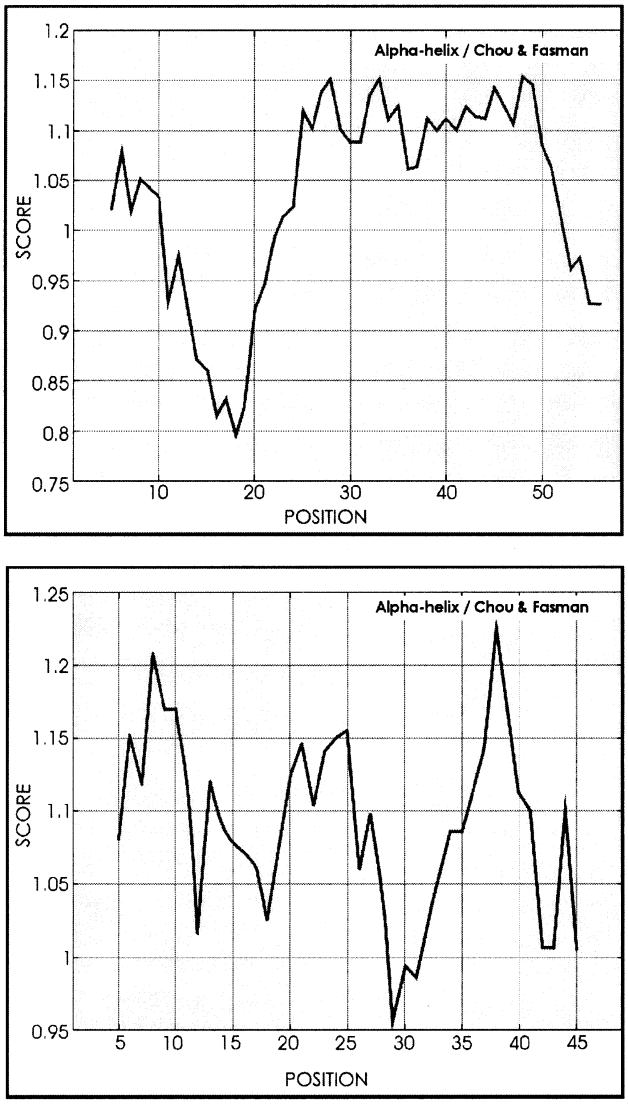

Figure 10. ProtScale conformational analysis for C-terminal divergent regions. This figure illustrates the ProtScale output for the wild-type (right) and mutant (left) terminal sequences. It can be seen from these graphs that the murine mutant terminus again has a higher predicted helical content (more structured) over the predicted helical content for the murine wild-type protein in this C-terminal region (8.07% versus 1.31%) (37–42). Taken together, these predictive techniques indicate that the mutant protein produced with its amino acid variation from the RDS wild-type, has a more highly structured C-terminal domain than the wild-type. Attempts to generate homology structures using both the SwissProt homology engine and Imperial Cancer Pssm threading engines were unsuccessful because of the absence of available structural homologues for the RDS protein.

observation that some RDS–peripherin mutants cause rod photoreceptors to degenerate while other mutations bring about the degeneration of cone photoreceptor cells (29). The presence of approximately 50 different mutations within the RDS–peripherin gene alone has stimulated the exploration of methods of generating therapeutic solutions that are independent of specific mutations. Such solutions can be targeted to the primary genetic defect, in this case the RDS–peripherin gene, or alternatively to a secondary effect associated with the pathology, such as apoptosis (programmed cell death). In this regard, it is of note that the rds-307 animal model generated in the current study will be useful for both purposes. Preliminary histological analyses of rds-307 mouse retinas suggests that while the primary stimulus for the disease is mutant peripherin, photoreceptors in rds-307 mice die by a process of apoptosis (Fig. 4D). Therefore this new animal model should be of value in the evaluation of various anti-apoptotic or neuroprotective approaches for therapy for inherited retinopathies (30–33). However, an alternative approach (or one that may be used in conjunction with the former) is to target the primary genetic defect, that is, the RDS–peripherin mutant in a mutation-independent manner. Technologies exploiting inherent features of the genome such as the degeneracy of the genetic code enable the development of such mutation-independent therapeutics (6–9) while still targeting the primary genetic defect. These approaches involve suppression of the mutant and wild-type alleles of the RDS–peripherin gene and in parallel the supply of a replacement RDS–peripherin gene that is protected from suppression but encodes wild-type protein (9). The novel mouse model (rds-307) described here, given the dominant-negative effect of the mutant, should be valuable in the exploration of such mutation-independent strategies (Table 1). A comparison between human RDS–peripherin and mouse rds–peripherin nucleotide sequences reveals that there are regions of mouse rds–peripherin sequences for which suppression agents such as hammerhead ribozymes could be designed and that would in principle be of relevance to the human disease, since the sequences at the ribozyme target site are almost identical between mouse and humans. Notably, five areas of such sequence homology exist in predicted open-loop structures of human RDS–peripherin and mouse rds–peripherin transcripts that could serve as targets for ribozymes that could be tested in rds-307 mice but in principle would also be applicable to suppression of the human gene (Table 1). Hence, in summary, the newly generated rds-307 mouse model described here will be of value in the evaluation of a variety

Table 1. Comparative analyses of human RDS–periperin and mouse rds–peripherin sequence illustrating co-targetable ribozyme cleavage sites

Position of cleavage site		Nucleotide sequence around ribozyme cleavage site
Human	306–308	5′-CCCAAGGGCTCTGGCTCATG-3′
Mouse	270–272	5′-CCCAGGGGCTCTGGCTTATG-3′
Human	582–584	5′-AACATCATCCTCTTCCTTGTG-3′
Mouse	546–548	5′-AACGTCATCCTCTTCCTGGTG-3′
Human	975–977	5′-ACGGAGGAGCTCAACCTGTGG-3′
Mouse	939–941	5′-ACTGAGGAGCTCAACCTCTGG-3′
Human	1050–1052	5′-ATGGGTGTCGTCACGCTCCTC-3′
Mouse	1014–1016	5′-ATGGGCGTCGTCACACTTCTC-3′
Human	1047–1049	5′-TCCATGGGTGTCGTCACGCTC-3′
Mouse	1011–1013	5′-TCCATGGGCGTCGTCACACTT-3′

Ribozymes have been designed so that they can simultaneously be used to cleave either human or mouse peripherin transcripts. Furthermore, each ribozyme cleavage site occurs at a degenerate position in human and mouse peripherin sequences so that mutation-independent suppression and replacement may be achieved. In addition, ribozyme cleavage sites are located in open-loop structures in both transcripts (as predicted from RNA secondary structures generated by RNA PlotFold). NUX ribozyme cleavage sites are highlighted in bold; mismatches between human and mouse peripherin sequences are underlined.

of therapeutic strategies of the sort described above, irrespective of whether the therapy targets the primary genetic defect or secondary effects associated with the disease pathology. In conclusion, in the current study, the first targeted mouse model of a peripherin-linked retinal degeneration has been generated. It has been clearly demonstrated that the resulting mouse has a significant photoreceptor degeneration. Notably, this new mouse model will be of value both in deciphering mechanisms of disease pathology and in exploring novel therapies for this group of retinal conditions.

MATERIALS AND METHODS

A 17 kb clone was isolated from a lambda dash phage library containing 129Sv-derived mouse genomic DNA (kindly donated by Dr Mario Capecchi) using PCR primers designed in the 5′ region of the mouse rds–peripherin gene. The insert was removed from lambda dash and cleaved into two fragments of 5 and 12 kb by digestion with SalI and SpeI restriction enzymes. These fragments were subcloned into pBluescript II $KS^{+/-}$. The 5 kb rds clone included exon III of the rds–peripherin gene. A 1 bp deletion at codon 307 known to occur in an autosomal dominant RP patient (34) was introduced into exon III of the gene by PCR mutagenesis. The construct was cloned into pPNT (kindly donated by Dr Andras Nagy), a vector that contains a HSV thymidine kinase (tk) gene suitable for negative selection. The pPNT vector was digested with the restriction enzymes XbaI and XhoI and ligated with the mutagenized 5 kb rds–peripherin fragment that had been removed from pBluescript II $KS^{+/-}$ by double digestion with SpeI and SalI. The neomycin resistance gene (plox neo) required for positive selection was cloned into an HpaI site (approximately 500 bp away from the 307 mutation) in the 3′ untranslated region of the rds–peripherin gene. The neomycin gene flanked by plox sites was removed from the ploxPneo-1 plasmid by digestion with XhoI and SmaI. Vector DNA was linearized with the NotI restriction enzyme. Linearized DNA was electroporated into R1 embryonic stem (ES) cells and positive/negative selection was used to enrich for targeted ES cell clones (G418 positive selection, gancyclovir negative selection). DNA from 32 selected ES cell clones was digested with XbaI and subjected to Southern analysis (Fig. 11). A 500 bp 3′ flanking PCR fragment was used as a probe to detect a 5.01 kb endogenous fragment that downshifted by approximately 1.17 kb to 4.18 kb in the targeted allele (Fig. 11C). Of the 32 selected clones, 8 were shown to possess the expected targeted allele.

Generation of chimeric mice

Selected ES colonies were injected into blastocysts of C57 Bl/6J mice to produce germline chimeras, which transmitted the RDS-307 mutation. Targeted RDS-307 mice were identified by PCR, sequencing and Southern blot analysis (Fig. 11). Mice that were heterozygous and homozygous for the RDS-307 gene mutation, were generated through inbreeding of germline-transmitting mutants, wild type litter mates were used as controls. The rds mice used throughout this study were Balb/c –rds/rds mice kindly supplied by Dr Richard L. Sidman.

Genotype assignments

PCR and sequencing techniques were used to identify mouse genotypes resulting from this breeding protocol. Oligo a (5′-GCA GAG AGT ATC AGA TGT TG-3′) is a forward primer for the rds–peripherin gene. Oligo b (5′-CAC ATA CAC TTC ATT CTC AG-3′) is a reverse primer for plox neo. A 25 µl PCR reaction mix contained 100 ng DNA, 50 pmol forward and reverse primers, 200 mM each of dGTP, dATP, dTTP and dCTP, 1.5 mM $MgCl_2$, 100 mM Tris, pH 9, 50 mM KCl, 1 × Triton X-100 and 0.75 U Taq polymerase. PCR conditions were 94°C, 1 min; 55°C, 1 min; 72°C, 1.2 min; 35 cycles. PCR products were resolved on a 2% agarose gel, a fragment of 1 kb being diagnostic of an allele containing the neomycin insert. To verify the presence of the 1 bp deletion, the above PCR product was sequenced across exon 3 using the primer oligo c (5′-GCC TCA TGT CTG CTC TAA GT-3′). An Applied Biosystems DNA sequencing kit and a 373 A DNA sequencer (Applied Biosystems) were used for this purpose.

Detection of the 1 bp 307 peripherin deletion in mRNA purified from retinas of rds-307 mice

Primer sequences to PCR-amplify exon 3 of the mouse peripherin cDNA (NM 008938) are (forward) GCTGGA-GAGTGTGTCTAACC and (reverse) TCCACCTGATT-GCTCTTGCC. The amplified sequence is 131 bp long in wild-type mice and 130 bp long in RDS-307 homozygous mice, and corresponds to the 1079–1210 bp sequence of NM 008938. The reverse primer was 5′ end-labeled with 6-FAM in order to enable detection in the ABI 310. DNA amplifications were undertaken using 100 ng genomic DNA (tail), 200 µM dNTPs, 1.5 mM $MgCl_2$, 5 pmol of each primer and standard PCR conditions for 32 cycles. RNAs were purified from retinas of 7-day-old animals using standard protocols (35). Approximately 2 µg RNA samples were DNase-treated (2 µl of RQ1 DNase, Promega) for 30 min at 37°C. RNA was subsequently phenol/chloroform-extracted and precipitated. One-third of the purified RNA samples (approximately 0.5 µg RNA) were used in subsequent RT reactions using a Qiagen RT kit (Omniscript reverse transcriptase) with either random hexamer or specific priming (2.5 pmol primer) in 20 µl reactions at 37°C for 1 hour. Control reactions were prepared by omitting Omniscript. From 1 to 3 µl of the RT reactions and controls (DNA controls) were used as template DNAs for subsequent PCR amplifications. PCR conditions used were the same as those described above for DNA amplifications. PCR products were diluted 1/50–150; 1 µl of the diluted sample was added to 12 µl of template suppression reagent (ABI) and denatured at 95°C for 5 min. An internal size standard 0.3 µl of GeneScan 400 HD (ABI) was also used. Samples were subsequently separated and sized on the ABI 310 genetic analyzer.

Histology

Eyes were perfused overnight with a mixture of 2.5% glutaraldehyde and 2% paraformaldehyde in 0.1 M phosphate buffer, pH 7.4, and processed in Epon (36). Sections 1 mm thick were cut through the optic nerve head, along the vertical

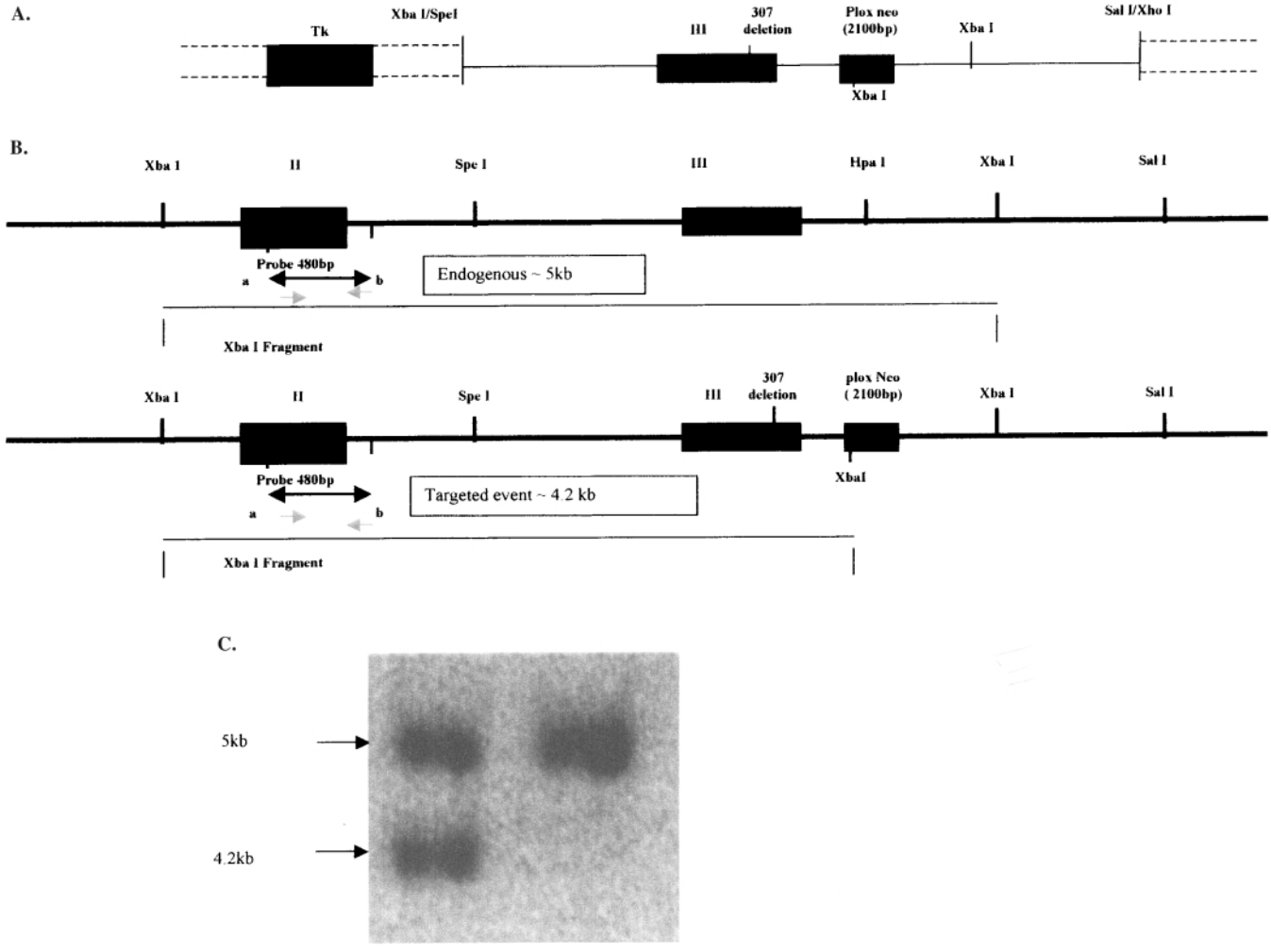

Figure 11. Construction of rds–peripherin Δ307 gene targeting vector. (A) Targeting vector (see Materials and Methods). (B) Restriction map illustrating plox neo insertion into the 3′ UTR and the 1 bp deletion at codon 307 in exon III, resulting in a 0.8 kb shift down in Southern blots; DNAs were digested with XbaI (C). The probe (probe 480) used for Southern blotting and the primers used to generate it are highlighted in green.

meridian of the eye, and were stained with toludine blue for light microscopy. The block was further trimmed and thin sections were cut. These sections were stained with uranyl acetate and lead citrate for electron microscopy.

Electroretinography

Animals were dark-adapted overnight and prepared for ERG under dim red light. Animals were anesthesized by means of ketamine and xylazine. Pupillary dilatation was achieved by instillation of atropine 0.1% and phenylephrine HCl 2.5%. Standardized flashes of light were presented to the mouse in a Ganzfeld bowl to ensure uniform retinal illumination. The ERG responses were recorded simultaneously from both eyes by means of gold wire loops on the corneas, using amethocaine 1% as topical anaesthesia and methylcellulose to maintain corneal hydration. A gold reference electrode was positioned subcutaneously approximately 1 mm from the temporal canthus and the ground electrode was placed subcutaneously anterior to the tail. The responses were analyzed using RetiScan RetiPort electrophysiology equipment (Roland Consulting Gmbh). The protocol used was based on that approved by the International Clinical Standards Committee for human electroretinography. Rod-isolated responses were recorded using a dim white flash (25 dB maximal intensity) presented in the dark-adapted state. The maximal combined rod/cone response to the maximal-intensity flash ($3\,cd\,m^{-2}\,s^{-1}$) was then recorded. Following light adaptation for 10 min to a background illumination of $30\,cd\,m^{-2}$ presented in the Ganzfeld bowl, the cone-isolated responses were recorded to both single-flash and 10 Hz maximal-intensity flashes. a-waves were measured from the baseline to the trough and b-waves from the baseline (in the case of rod-isolated responses) or from the a-wave trough.

ACKNOWLEDGEMENTS

We wish to express our sincere thanks to Dr Andras Nagy for valued advice and assistance in the development of embryonic stem cell technology and the generous provision of targeting vectors. We also thank Dr Jim Curry and Dr John Findlay for

helpful comments and discussion. We are grateful to Eileen Rattner, Brenda Carson, Jeannine Turnbull, Mary Phillips and Caroline Woods for their technical support and animal care. The graphic skills of Dr Avril Kennan are also much appreciated. This research has been supported by grants from the Wellcome Trust, Foundation-Fighting Blindness (USA), British RP Society, Fighting Blindness Ireland, The Health Research Board of Ireland and the European Union 5th Framework program. The Ocular Genetics Unit at TCD is a member of HEA-sponsored Biopharmaceutical Sciences network.

REFERENCES

1. Molday, R.S. (1998) Photoreceptor membrane proteins, phototransduction, and retinal degenerative diseases. Invest. Opthalmol. Vis. Sci., 39, 2493–2513.
2. Humphries, P., Kenna, P. and Farrar, G.J. (1992) On the molecular genetics of retinitis pigmentosa. Science, 256, 804–808.
3. Farrar, G.J., Kenna, P., Jordan, S.A., Kumar-Singh, R., Humphries, M.M., Sharp, E.M., Sheils, D.M. and Humphries, P. (1991) A three-base-pair deletion in the peripherin-RDS gene in one form of retinitis pigmentosa. Nature, 354, 478–480.
4. Farrar, G.J., Kenna, P., Redmond, R., Shiels, D., McWilliam, P., Humphries, M.M., Sharp, E.M., Jordan, S., Kumar-Singh, R. and Humphries, P. (1991) Autosomal dominant retinitis pigmentosa: a mutation in codon 178 of the rhodopsin gene in two families of Celtic origin. Genomics, 4, 1170–1171.
5. Kajiwara, K., Hahn, L.B., Mukai, S., Travis, G.H., Berson, E.L. and Dryja, T.P. (1991) Mutations in the human retinal degeneration slow gene in autosomal dominant retinitis pigmentosa. Nature, 354, 478–480.
6. Millington-Ward, S., O'Neill, B., Tuohy, G., Al-Jandal, N., Kiang, A.S., Kenna, P.F., Palfi, A., Hayden, P., Mansergh, F., Kennan, A. et al. (1997) Strategems in vitro for gene therapies directed to dominant mutations. Hum. Mol. Genet., 9, 1415–1426.
7. Millington-Ward, S., O'Neill, B., Kiang, A.S., Humphries, P., Kenna, P.F. and Farrar, G.J. (1999) A mutation-independent therapeutic strategem for osteogenesis imperfecta. Antisense Nucleic Acid Drug Dev., 9, 537–542.
8. O'Neill, B., Millington-Ward, S., O'Reilly, M., Tuohy G., Kiang, A.S., Kenna, P.F., Humphries, P. and Farrar, G.J. (2000) Ribozyme-based therapeutic approaches for autosomal dominant retinitis pigmentosa. Invest. Ophthalmol. Vis. Sci., 41, 2863–2869.
9. Farrar, G.J., Kenna, P.F., and Humphries, P. (2002) New EMBO members review: On the genetics of retinitis pigmentosa and on mutation-independent approaches to therapeutic intervention. EMBO J., 21, 857–864.
10. Arikawara, K., Molday, L.L., Molday, R.S. and Williams, D.S. (1992) Localization of peripherin/rds in the disk membranes of cone and rod photoreceptors: relationship to disk membrane morphogenesis and retinal degeneration. J. Cell. Biol., 116, 659–667.
11. Bascom, R.A., Manara, S., Collins, L., Molday, R.S., Kalnins, V.I. and McInnes, R.R. (1992) Cloning of the cDNA for a novel photoreceptor membrane protein (rom-1) identifies a disk rim protein family implicated in human retinopathies. Neuron, 6, 1171–1184.
12. Moritz, O.L. and Molday, R.S. (1996) Molecular cloning, membrane topology, and localization of bovine rom-1 in rod and cone photoreceptor cells. Invest. Ophthalmol. Vis. Sci., 37, 352–362.
13. Goldberg, A.F. and Molday, R.S. (2000) Expression and characterisation of peripherin/rds-rom-1 complexes and mutants implicated in retinal degenerative diseases. Meth. Enzymol., 316, 671–687.
14. Sanyal, S., De Ruiter, A. and Hawkins, R.K. (1980) Development and degeneration of retina in rds mutant mice: light microscopy. J. Comp. Neurol., 194, 193–207.
15. Sanyal, S. and Jansen, H.G. (1981) Absence of receptor outer segments in the retina of rds mutant mice. Neurosci. Lett., 21, 23–26.
16. Connell, G., Bascom, R., Molday, L., Reid, D., McInnes, R.R. and Molday, R.S. (1991) Photoreceptor peripherin is the normal product of the gene responsible for retinal degeneration in the rds mouse. Proc. Natl Acad. Sci. USA, 88, 723–726.
17. Gruning, G., Millan, J.M., Meins, M., Beneyto, M., Caballero, M., Apfelstedt-Sylla, E., Theischen, M., Ruther, K., Wedemann, H., Gal, A. and Zrenner, E. (1994) Extensive intrafamilial and interfamilial phenotypic variation among patients with autosomal dominant retinal dystrophy and mutations in the human RDS/peripherin gene. Br. J. Ophthalmol., 79, 28–34.
18. Kedzierski, W., Lloyd, M., Birch, D.G., Bok, D. and Travis, G.H. (1997) Generation and analysis of transgenic mice expressing P216L-substituted Rds/peripherin in rod photoreceptors. (1997) Invest. Opthalmol. Vis. Sci., 38, 498–509.
19. Kedzierski, W., Nusinowitz, S., Birch, D., Clarke, G., McInnes, R.R., Bok, D. and Travis G.H. (2001) Deficiency of rds/peripherin causes photoreceptor death in mouse models of digenic and dominant retinitis pigmentosa. Proc. Natl Acad. Sci. USA, 8, 7718–7723.
20. Jansen, H.G. and Sanyal, S. (1992) Synaptic plasticity in rod terminals after partial photoreceptor cell loss in the heterozygote rds mutant mouse. J. Comp. Neurol., 316, 117–125.
21. Sanyal, S., Dees, C. and Zeilmaker, G.H. (1986) Development and degeneration of retina in rds mutant mice: observations in chimaeras of heterozygous mutant and normal genotype. J. Embryol. Exp. Morphol., 98, 111–121.
22. Nagy, A. (2000) Cre recombinase: the universal reagent for genome tailoring. Genesis, 26, 99–109.
23. Connell, G.J. and Molday, R.S. (1990) Molecular cloning, primary structure, and orientation of the vertebrate photoreceptor cell protein peripherin in the rod outer segment disk membrane. Biochemistry, 29, 4691–4698.
24. Molday, R.S. (1994) Peripherin/rds and rom-1: molecular properties and role in photoreceptor degeneration. Prog. Ret. Eye Res., 13, 271–298.
25. Tam, B.M., Moritz, O.L., Hurd, C.B. and Papermaster, D.S. (2001) Are the COOH terminal regions of rod outer segment proteins potential targeting signals? Invest. Ophthalmol. Vis. Sci., 42, S365.
26. Boesze-Battaglia, K., Lamba, O.P., Napoli, A, Jr, Sinha, S. and Guo, Y (1998) Fusion between retinal rod outer segment membranes and model membranes: a role for photoreceptor peripherin/rds. Biochemistry, 37, 9477–9487.
27. Wrigley, J.D.J., Ahmed, T., Nevett, C.L., and Findlay, J.B.C. (2000) Peripherin/rds influences membrane vesicle morphology. J. Biol. Chem., 275, 13191–13194.
28. Cuff, J.A., Clamp, M.E., Siddiqui A.S., Finlay, M. and Barton G.J. (1998) Jpred: a consensus secondary structure prediction server. Bioinformatics, 14, 892–893.
29. Jacobson, S.G., Cideciyan, A.V., Maguire, A.M., Bennett, J., Sheffield, V.C. and Stone, E.M. (1996) Preferential rod and cone photoreceptor abnormalities in heterozygotes with point mutations in the RDS gene. Exp. Eye Res., 63, 603–608.
30. Davidson, F.F. and Stellar H. (1998) Blocking apoptosis prevents blindness in Drosophila retinal degeneration mutants. Nature, 391, 587–591.
31. Liu, C., Li, Y., Peng, M., Laties, A.M. and Wen, R. (1999) Activation of caspase-3 in the retina of transgenic rats with the rhodopsin mutation s334ter during photoreceptor degeneration. J. Neurosci., 19, 4778–4785.
32. Eversole-Cire, P., Concecion, F.A., Simon, M.I., Takayama, S., Reed, J.C. and Chen, J. (2000) Synergistic effect of Bcl-2 and BAG-1 on the prevention of photoreceptor cell death. Invest. Ophthalmol. Vis. Sci., 41, 1953–1961.
33. Nir, I., Kedzierski, W., Chen, J. and Travis, G.H. (2000) Expression of Bcl-2 protects against photoreceptor degeneration in retinal degeneration slow (rds) mice. J. Neurosci., 20, 2150–2154.
34. Gruning, G., Millan, J.M., Meins, M., Beneyto, M., Caballero, M., Apfelstedt-Sylla, E., Bosch, R., Zrenner, E., Prieto, F. and Gal, A. (1994) Mutations in the human peripherin/RDS gene associated with autosomal dominant retinitis pigmentosa. Hum. Mutat., 3, 321–323.
35. Kennan, A., Aherne, A., Palfi, A., Humphries, M., Stitt, A., Simpson, D.A.C., Demptroeder, K., Orntoff, T., Ayuso, C., Kenna, P.F. et al. (2002) Identification of an IMPDH1 mutation in autosomal dominant retinitis pigmentosa (RP10) revealed following comparitive microarray analysis of transcripts derived from retinas of wild-type and Rho$^{-/-}$ mice. Hum. Mol. Genet., 11, 547–557.
36. Humphries, M.M., Rancourt, D., Farrar, G.J., Kenna, P., Hazel, M., Bush, R.A., Sieving, P.A., Sheils, D.M., McNally, N., Creighton, P. et al. (1997) Retinopathy induced in mice by targeted disruption of the rhodopsin gene. Nature Genet., 15, 216–219.
37. Chou, P.Y. and Fasman, G.D. (1978) Amino acid scale: conformational parameter for alpha helix. Adv. Enzymol., 47, 45–148.

38. Muñoz, V. and Serrano, L. (1994) Elucidating the folding problem of α-helical peptides using empirical parameters. Nature Struct. Biol. 1, 399–409.
39. Muñoz, V. and Serrano, L. (1994) Elucidating the folding problem of α-helical peptides using empirical parameters, II. Helix macrodipole effects and rational modification of the helical content of natural peptides. J. Mol. Biol., 245, 275–296.
40. Muñoz, V. and Serrano, L. (1994) Elucidating the folding problem of α-helical peptides using empirical parameters, III. Temperature and pH dependence. J. Mol. Biol., 245, 297–308.
41. Muñoz, V. and Serrano, L. (1997) Development of the multiple sequence approximation within the Agadir model of α-helix formation. Comparison with Zimm-Bragg and Lifson–Roig formalisms. Biopolymers, 41, 495–509.
42. Lacroix, E., Viguera, A.R. and Serrano, L. (1998) Elucidating the folding problem of α-helices: local motifs, long-range electrostatics, ionic strength dependence and prediction of NMR parameters. J. Mol. Biol., 284, 173–191.